

Long-term stable transmission of 3-keV Ne⁷⁺ ions guided through nanocapillaries in polymers



N. Stolterfoht^{a,*}, P. Herczku^b, Z. Juhász^b, S.T.S. Kovács^b, R. Rácz^b, S. Biri^b, B. Sulik^b

^a Helmholtz-Zentrum Berlin für Materialien und Energie, 14109 Berlin, Germany

^b Institute of Nuclear Research (ATOMKI), 4001 Debrecen, Hungary

ARTICLE INFO

Article history:

Received 21 August 2016

Received in revised form 6 October 2016

Accepted 7 October 2016

Available online 14 October 2016

Keywords:

Capillary guiding

Ion transmission

Nanocapillaries

Highly charged

Areal density

ABSTRACT

We studied blocking effects on 3-keV Ne⁷⁺ ion guiding through nanocapillaries in highly insulating polyethylene terephthalate (PET) manufactured at different laboratories. The experiments were motivated in view of previous measurement with PET capillaries prepared at the GSI Helmholtz-Zentrum for which significant blocking effects were observed, whereas in various previous studies with PET capillaries these effects could not be detected. As the blocking effect on the GSI capillaries strongly depends on their areal density, similar dependencies were studied with the FLNR capillaries. Long-term stable transmission was observed for all densities of the FLNR capillaries in contrast to the previous results. These observations are interpreted by differences in the capillary surface conductivities in accordance with charge patch formations within the capillaries. It is pointed out that the observed stable transmission is favorable for applications of ion guiding in capillaries.

© 2016 Elsevier B.V. All rights reserved.

1. Introduction

Since ion guiding through insulating capillaries with a diameter of a hundred nanometer has been observed [1], the subject received considerable attention. Such nanocapillaries in highly insulating materials accumulate ions at the wall so that charge patches are created. The charge patch in the capillary entrance region produces a repulsive electric field, which deflects subsequent ions to the exit. The ion deflection occurs at relatively large distances from the capillary wall, which inhibits electron capture into the projectile. Thus, the ions incident into a tilted capillary can be guided along the capillary axis maintaining their incident charge state. The outstanding property of ion guiding is the self-organizing process, which governs the charge patch formation and the ion transmission through the capillaries.

Initial studies of ion guiding phenomena in insulating materials have been performed using capillaries in polyethylene terephthalate (PET) [1–3]. As the interest in this field increased, several laboratories performed similar experiments. Besides further studies with PET [4–8] other materials were used such as polycarbonate (PC) [9–12], SiO₂ [13,14], Al₂O₃ [15–17], and mica [18]. Moreover, ion guiding was studied with single capillaries of constant diameter [19,20] and of tapered geometry to produce sub-micrometer

sized ion beams [21,22]. Apart from the experimental work, a series of theoretical studies [23–26] has provided detailed information about the guiding mechanisms. Additional investigations with keV ions and other projectiles, such as electrons, are presented in recent reviews [27,28].

In previous work particular attention has been devoted to the time evolution of the ion fraction guided through capillaries. Oscillatory structures have been observed for the mean emission angle of the transmitted ions [14,29]. The oscillations can be associated with the transient formation of secondary charge patches. Apart from the dominant charge patch near the entrance region, additional weaker patches are temporarily produced further inside the capillaries as shown in Fig. 1(a). At equilibrium, the secondary patches lose importance as indicated in Fig. 1(b). Temporary charge patches can only be formed when the charge removal is limited. Thus, the charge patch formation provides information about the capillary surface conductivity.

For non-zero tilt angles the ion transmission usually starts with a time delay and then rises to a maximum where stationary (equilibrium) conditions are expected to be maintained. In early studies with PET [1–3,5] the fraction of transmitted ions were observed to remain constant after reaching the maximum transmission. Only recently, experiments with PC capillaries have shown that after reaching a maximum the transmitted ion fraction decreases with increasing charge insertion [11,12]. In recent years, this observation has been referred to as blocking of the ion transmission. It

* Corresponding author.

E-mail address: nico@stolterfoht.com (N. Stolterfoht).

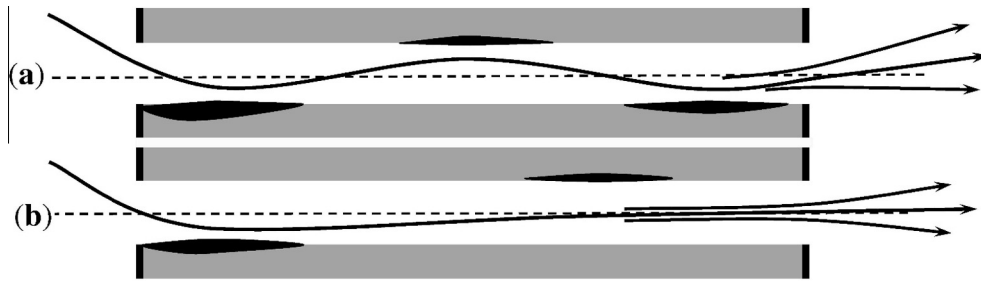


Fig. 1. Schematics of ion guiding through capillaries by charge patches indicated by black spots [25]. Graphs (a) and (b) show typical trajectories occurring in, respectively, the dynamic and the equilibrium period of the charge evolution.

should be noted that this blocking effect was observed for 3 keV Ne^{7+} ions, whereas in previous studies [10] using 10–40 keV Ne^{7+} blocking did not occur for PC capillaries. Thus, blocking can be avoided by using higher energies of the projectiles for which, however, the guiding effect loses importance [10].

In the experiments with 3 keV Ne^{7+} ions the capillaries in PC had an areal density which was an order of magnitude larger than that of the capillaries in PET [11]. Hence, the question arose whether the blocking was produced by density effects or material properties. Therefore, further measurements were performed with PET [30] as a function of the areal capillary density. The results clearly indicated that blocking effects are significant for higher areal densities of $\sim 6 \times 10^7 \text{ cm}^{-2}$. Thus, it was concluded from the experiments and also from model calculations that blocking of ion guiding sensitively depends on the areal density of the capillaries. (It is noted, however, that the model calculations are based on the limiting case of zero conductivity within the capillaries.) The similar results for the capillary materials PC [11] and PET [30], suggested the possible conclusion that ion blocking is a general phenomenon for high density capillaries.

With this observation, the open question remained why before the recent work [11] blocking effects have never been observed for PET capillaries. In this context it should be noted that the previous measurements with PET were generally conducted for a limited charge insertion into the capillaries. Furthermore, the PET capillaries, which showed blocking [30] were prepared at the GSI Helmholtz-Zentrum in Darmstadt (Germany) [31] and the capillaries, which suggested stable transmission (e.g., [5]) were manufactured at a different laboratory, i.e., the Flerov Laboratory of Nuclear Reaction (FLNR) in Dubna (Russia) [32]. In the following, the two laboratories will be referred to as GSI and FLNR, respectively.

To obtain decisive information about blocking effects, we studied guiding of 3-keV Ne^{7+} through FLNR PET capillaries using a significant charge insertion and an areal density, which was higher than that applied previously. In contrast to the previous GSI PET experiments [30], the present results revealed stable unblocked transmission for the high capillary density of $1 \times 10^8 \text{ cm}^{-2}$ and charge insertion as large as 40 fC per capillary. From the experimental results it follows that ion blocking is not a general rule for high density capillaries.

2. Experimental method

The experiment was carried out at the Institute of Nuclear Research of the Hungarian Academy of Sciences (ATOMKI), Debrecen. Highly charged ions were provided by an electron cyclotron resonance (ECR) ion source [33], which was operated with an extraction voltage of 429 V to produce 3 keV Ne^{7+} . The beam was collimated by two diaphragms of 0.5 mm diameter spaced 20 cm apart before entering the experimental chamber. This restricted the beam divergence to 0.2° FWHM (full width at half maximum),

whose current was typically 100 pA. In the experimental chamber, where the target sample and the detector were placed, the vacuum was $\sim 8 \times 10^{-7}$ mbar. More details about the experimental arrangement can be found in Ref. [17].

The final charge state of the ion that passed through a capillary, could be selected using an electric deflection field in front of the ion detector. In particular, it was shown that the amount of neutrals within the ion beam is minor. Also, we could show that the fraction of electrons is negligible within the ion beam hitting the target. The negligible fraction of electrons was revealed by comparing the ion beam current measured with an unbiased and negatively biased Faraday cup.

For the experiments, FLNR samples of PET were used with areal capillary densities of $4 \times 10^6 \text{ cm}^{-2}$ and $1 \times 10^8 \text{ cm}^{-2}$. These PET samples were initially prepared in Dubna by bombarding 250 MeV Kr ions on a PET membrane of 12 μm thickness. The membranes were further treated at the Ionenstrahl-Labor (ISL) in Berlin to produce capillaries by etching the ion tracks in a NaOH solution. Thus, capillaries with a diameter of 200 nm were produced and then utilized in experiments at ISL [5,6]. For the present measurements the FLNR capillary samples were finally transported from ISL to ATOMKI [8].

Fig. 2(a) and (c) displays images obtained with scanning electron microscopy (SEM) to show the areal capillary densities of $4 \times 10^6 \text{ cm}^{-2}$ and $1 \times 10^8 \text{ cm}^{-2}$, respectively. The density of the capillaries implies a geometric opening of 0.15% and 3%. Due to the stochastic nature of the ion beam the capillary entries are statistically distributed over the surface. The angular spread of the capillary inclination was estimated to be $\lesssim 0.2^\circ$ FWHM, which is significantly smaller than the aspect angle of 1° . Gold was evaporated under 30° on both the front and the back sides of the PET foil, forming a film of ~ 20 nm thickness to avoid a macroscopic charge up of the sample surfaces.

Since the present results will be compared with previous experiments [30] using GSI samples, a few details about these capillaries shall be given here. They were produced at the GSI Helmholtz-Zentrum in Darmstadt by irradiating 10 μm PET membranes with 2.2 GeV gold ions [31]. Samples were prepared with different capillary densities ranging from 3×10^6 to $6 \times 10^7 \text{ cm}^{-2}$. The irradiated foils were also etched by NaOH, converting ion tracks into capillaries with a diameter of ~ 140 nm. Examples of the capillary opening are given in Fig. 2(b) and (d) for areal densities of $5 \times 10^6 \text{ cm}^{-2}$ and $6 \times 10^7 \text{ cm}^{-2}$, respectively. Also, gold layers were evaporated on the front and the back sides of the PET foils.

The capillary samples were mounted on a goniometer, which allowed for an alignment in three axial dimensions and around one rotational axis. The PET membranes were spanned on a circular frame with an inner diameter of 7 mm. When a new measurement was started, the sample holder was shifted to localize the beam to a fresh spot on the target foil. Hence, previous charge-up effects could be avoided. In particular, a fresh spot was chosen when setting a new tilt angle ψ , which is equal to the angle

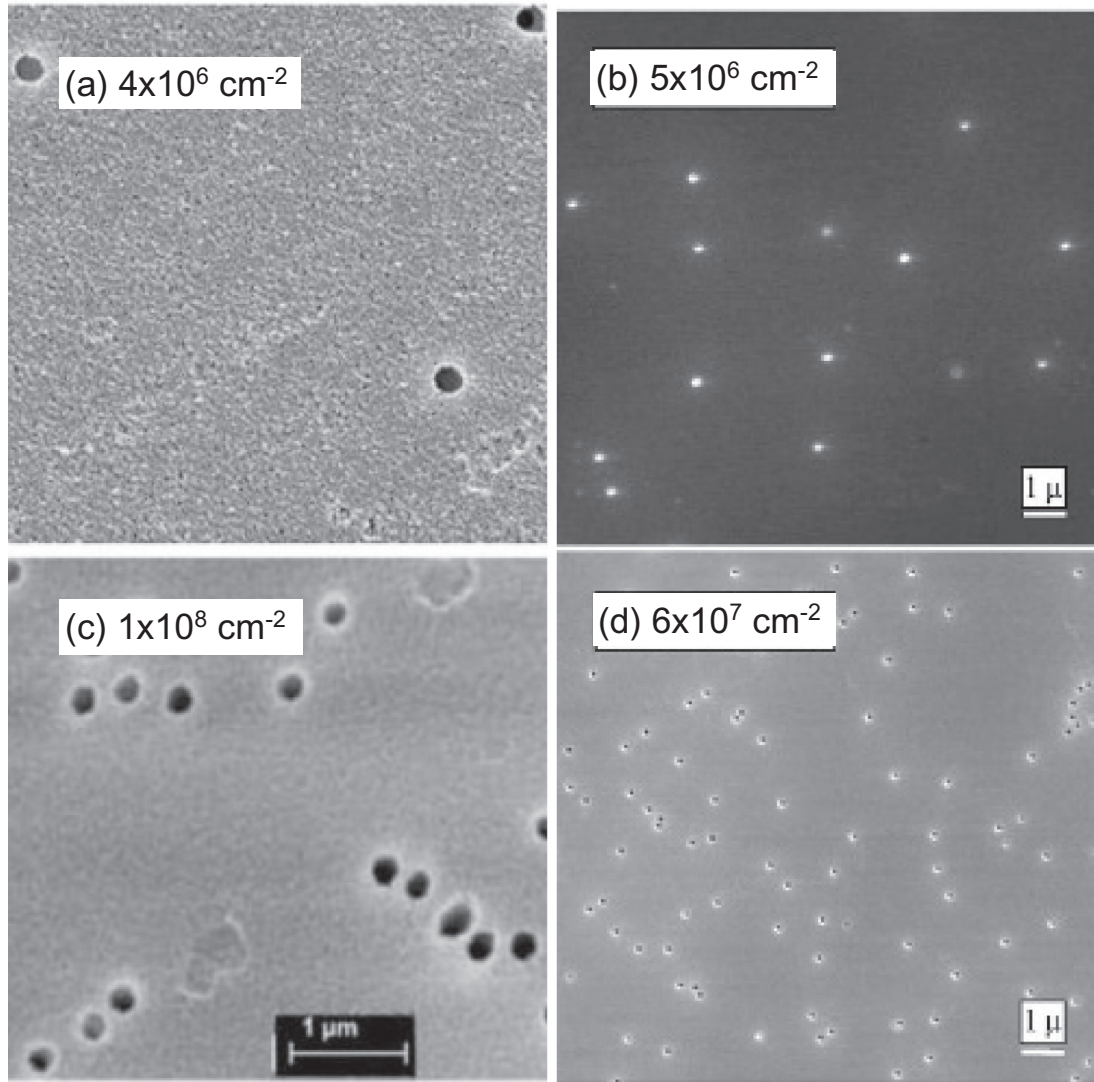


Fig. 2. Density plots presenting capillary openings obtained by means of scanning electron microscopy. In the left-hand column the panels (a) and (c) show capillaries with a diameter of 200 nm [5,6] prepared at FLNR. In the right-hand column the panels (b) and (d) show capillaries with a diameter of 140 nm manufactured at GSI [31]. Areal capillary densities are given in the individual panels.

between the capillary axis relative to the incident beam. While, the tilt angle could be changed, the azimuthal inclination was fixed close to zero degree. The value of the azimuthal angle was equal to $\phi \approx 0.8^\circ$ as estimated from the mean azimuthal angle of the transmitted beam.

The transmitted ions were observed using a multi channel plate detector (MCP) positioned 74 mm away from the capillary target keeping its surface parallel to that of the capillary foil. This was achieved by rotating the MCP around the same axis as the sample holder. Thus, the capillary axes always pointed to the center of the MCP detector. Two-dimensional images were collected in sequences of acquisition intervals of 9 s and breaks of 1 s between them. After each acquisition interval the measured MCP image and the charge Q_d deposited at the capillary sample was stored. Since the ion beam was quite constant in the present experiments (with fluctuation of less than 10%), the deposited charge can also be considered as a measure of time t .

Previous studies [5] have shown that the experimental results scale with the deposited charge rather than with time. In fact, instead of Q_d , the charge Q_{in} inserted per capillary is used to plot the transmitted ion fraction, which is advantageous when results for different capillary diameters are compared. The charge Q_{in} is

obtained by the relation $Q_{in} = Q_d(d/D)^2$, where d is the diameter of the capillary and D is the diameter of the ion beam (~ 0.8 mm).

3. Experimental results

3.1. Transmission profiles

In Fig. 3 we present series of MCP images of 3-keV Ne^{7+} ions transmitted through FLNR PET capillaries for tilt angles of 1.3° and 6° (here, -1.3° is replaced by 1.3° as the minus sign is irrelevant). Since a deflecting electric field was applied, the images of Ne^{7+} ions are free from other charge states. The position on the MCP was converted to angular coordinates indicated at the axes of the figures. The horizontal axis represents the angular deviations θ_x with respect to the beam (z axis) in the x-z plane while the vertical axis corresponds to the angle θ_y in the y-z plane. An image corresponds to the double differential angular distribution $dY(\theta_x, \theta_y)/d\Omega$, which is referred to as transmission profile. The tilt angle is varied along the horizontal axis moving the profile within the x-z plane.

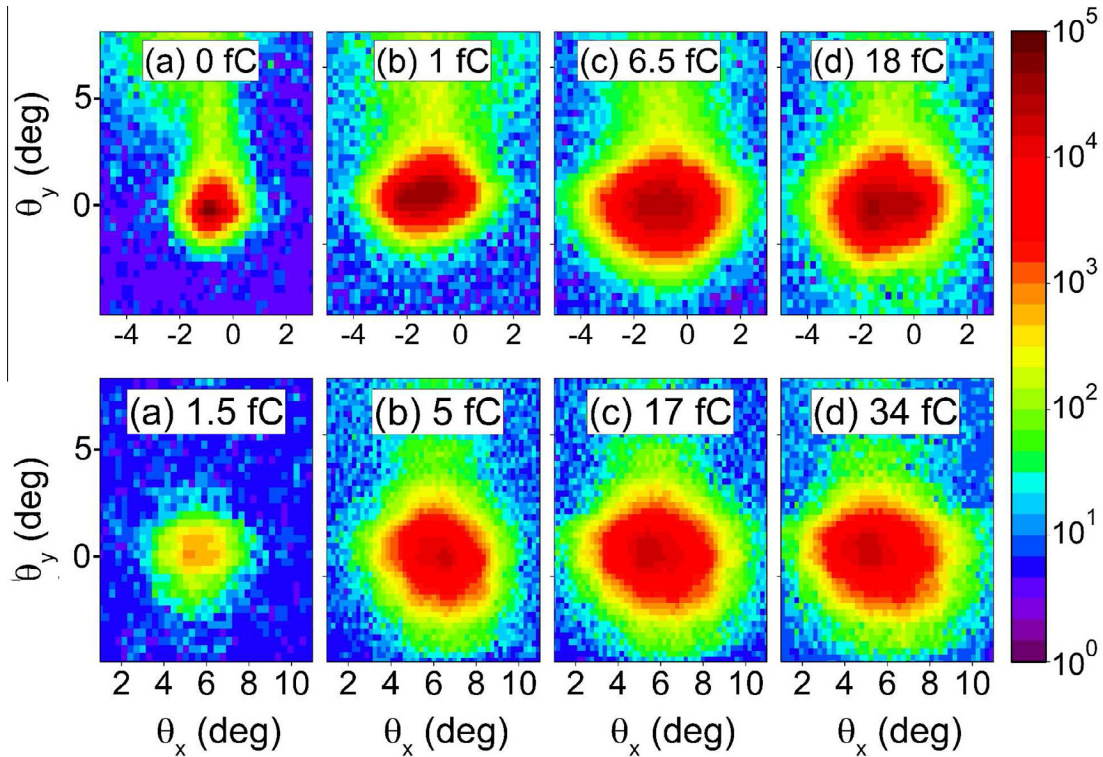


Fig. 3. Two-dimensional images of 3-keV Ne^{7+} ions transmitted through FLNR capillaries measured by the MCP detector at the tilt angle of -1.3° (upper row) and 6° (lower row). Ions with other charge states are removed from the images by an electric deflector field. Each panel indicates the charge Q_{in} inserted per capillary before the image is taken.

As mentioned, the data were taken within the time interval of 9 s after having inserted the charge Q_{in} indicated in each panel. Hence, the images represent a temporal evolution of the ion transmission. For the tilt angle of 1.3° the emission of Ne^{7+} is clearly visible from the beginning of the charge insertion as seen in Fig. 3(a). There, the Ne^{7+} emission profile is less intense and has a smaller width than those in the other panels. The increase of the profile width with increasing charge insertion is a well-known phenomenon that indicates the accumulation of the charge within the capillary [30]. This charge accumulation results from the non-zero tilt angle and the divergence of the ion beam.

The lower row of Fig. 3 shows MCP images of transmitted Ne^{7+} ions for the tilt angle of 6° . Again, the charge Q_{in} , inserted per capillary before the image was taken, is indicated in each panel. In the first panel labeled (a) the intensity of the transmitted Ne^{7+} ions is found to be weak. This is due to the delay of the entrance charge patch formation, which is responsible for the ion transmission. In the other panels (b)–(d) of the images are stable with respect to intensity and width.

3.2. Ion transmission yields

The total yield for the transmission of Ne^{7+} ions was determined by summing the counts within circular areas on the detector surface surrounding the corresponding center positions. Thus, we consider the total ion yield Y_t transmitted through the capillaries, which is obtained from the integration of the transmission profiles

$$Y_t = \int \frac{dY(\theta_x, \theta_y)}{d\Omega} d\Omega. \quad (1)$$

Shifting the areas away to signal free positions the background contribution was determined and subtracted.

In order to take into account beam current fluctuations the integrated counts were normalized to the charge deposited at the

sample during the acquisition. This process was repeated for each image recorded successively in time. As noted, for a given incident beam current the deposited charge is a measure of time.

Next, the temporal evolutions of 3-keV Ne^{7+} ion transmission through GSI and FLNR capillaries are compared. For each capillary type two samples were used with capillary densities differing by an order of magnitude. To allow for a convenient comparison of data obtained with different capillary densities, the total intensity Y_t from Eq. (1) was normalized by the number of ions Y_{in} inserted into all capillaries. Thus, the fraction of transmitted ions $f_t = Y_t/Y_{in}$ is obtained. The number of incident ions Y_{in} is proportional to the capillary density δ_c so that f_t contains a normalization by that density.

Fig. 4(a) shows the transmitted 3-keV Ne^{7+} ion fraction, obtained previously by means of a GSI capillary sample [30], whereas Fig. 4(b) presents the results for the FLNR capillaries measured in this work. The capillary diameters (140 nm and 200 nm) and tilt angles (0.2° and 5°) are given in the graphs. For both capillary types the areal densities are relatively low, i.e., equal to $5 \times 10^6 \text{ cm}^{-2}$. The ion fractions are plotted as a function of the charge Q_{in} inserted per capillary.

As the results for the GSI capillaries in Fig. 4(a) have previously been reported [30], only essential details shall be mentioned here. The curve exhibit a rapid increase at the beginning of the charge insertion, which can be attributed to small deviation of 0.2° from the zero degree tilt angle. The striking feature of the GSI capillary results is that after being essentially constant, the transmission curve starts to decrease by about a factor of two as Q_{in} rises from 26 to 38 fC. This decrease can be considered as the beginning of ion blocking.

In Fig. 4(b) the transmission curve for the FLNR capillaries is shown. The ion transmission starts at a threshold near 1 fC as is usual for a delayed charge patch formation [5]. After an increase of the transmission, an equilibrium value of 17% is achieved, which is typical for the tilt angle of 5° [6]. As mentioned, these capillaries

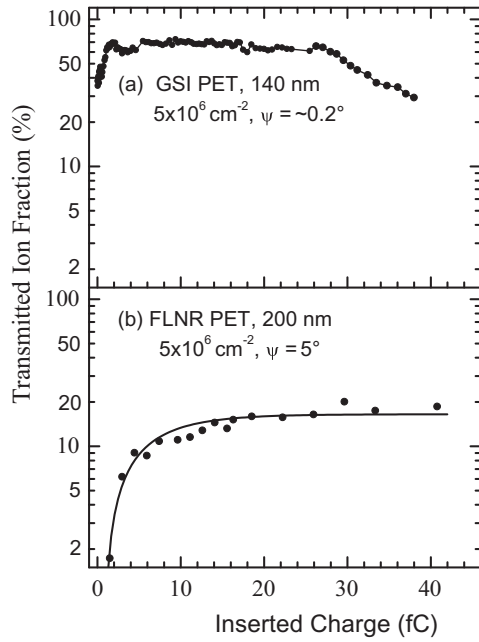


Fig. 4. Fraction f_t of 3-keV Ne^{7+} ions transmitted through PET capillaries plotted as a function of the inserted charge Q_{in} . In (a) results for a GSI sample are presented using a tilt angle of $\sim 0.2^\circ$ [30]. In (b) results for a FLNR sample are given for the tilt angle of 5° . The areal capillary densities are equal to $5 \times 10^6 \text{ cm}^{-2}$, as given in both panels.

have been used in previous experiments [5] yielding results similar as those given here. However, the data in Fig. 4(b) were measured for inserted charges, which are significantly larger than those reached before.

The important result of the FLNR sample is that the transmission curve remains constant for charge insertion up to $Q_{in} = 42 \text{ fC}$. Similar results have previously been obtained by low density FLNR capillaries with a diameter of 100 nm [11]. Thus, for the FLNR PET samples with a capillary density of $5 \times 10^6 \text{ cm}^{-2}$ no indication for ion blocking could be observed.

Next, we consider the ion transmission for capillaries with higher areal density. Fig. 5(a) shows results for a GSI sample [30] containing capillaries with a density of $6 \times 10^7 \text{ cm}^{-2}$, which is about a factor of 10 higher than that involved in Fig. 4(a). In Fig. 5(a) the transmission curve rises quickly, again due to the small deviation from the zero degree tilt angle. Then, after passing a steep maximum, the ion transmission decreases by more than an order of magnitude, which significantly differs from the behavior found for the low capillary density [Fig. 4(a)]. Hence, it has been concluded that the ion blocking in the GSI samples is mainly affected by the areal capillary density. The strong density dependence has been attributed to the influence of neighbor capillaries as shown by model calculations [30].

Fig. 5(b) depicts results from the FLNR sample for an enhanced capillary density of $1 \times 10^8 \text{ cm}^{-2}$. The data were obtained with a tilt angle of 2° and a capillary diameter of 200 nm (as before). It is seen that the transmission curve remains stable for a charge insertion as large as 45 fC . Hence, no blocking effects are observed for the FLNR capillary even for the relatively large areal density. In fact, the transmission curves for low and high capillary densities are practically equal [compare Fig. 4(b) with Fig. 5(b)]. This observation for the FLNR capillaries significantly differs from the corresponding results for the GSI samples [Fig. 4(a) with Fig. 5(a)].

To search for an explanation, one notes that the capillary types differ in diameter and tilt angle. It is not expected that the capillary diameter plays an important role for stable ion transmission. It should be recalled that nearly the same transmission curves were

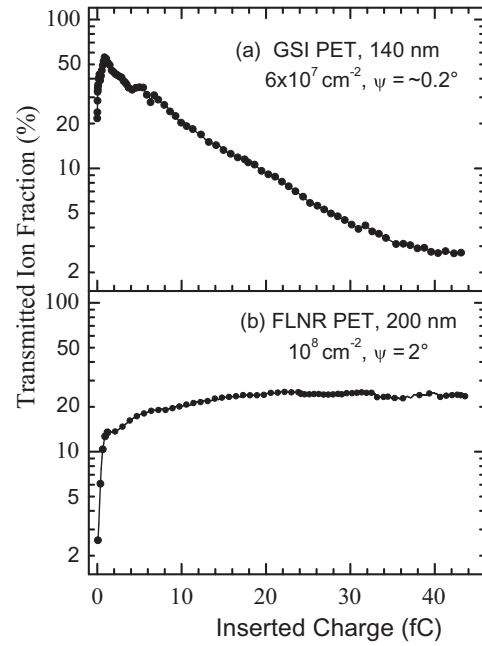


Fig. 5. Fraction f_t of 3-keV Ne^{7+} ions transmitted through PET capillaries plotted as a function of the inserted charge Q_{in} . In (a) results for a GSI sample are presented using a tilt angle of $\sim 0.2^\circ$ [30] and in (b) results for a FLNR sample are given for the tilt angle of 2° . The areal capillary densities are equal to $6 \times 10^7 \text{ cm}^{-2}$ and $1 \times 10^8 \text{ cm}^{-2}$, as given in panels (a) and (b), respectively.

observed for FLNR capillaries with diameters of 200 nm [Fig. 4(b)] and 100 nm [11]. However, blocking effects on PC capillaries have been found to increase with decreasing capillary tilt angle [11]. Therefore, we investigated the 3-keV Ne^{7+} ion transmission through the FLNR capillaries for different tilt angles.

Fig. 6 shows the ion transmission through FLNR capillaries with the high density of $1 \times 10^8 \text{ cm}^{-2}$. The transmission curves in panels (a), (b), and (c) are obtained with tilt angles of 1.3° , 2° , and 6° , respectively. The intensity for the tilt angle of 6° starts with a relatively large threshold of 2 fC , which can again be attributed to a delayed charge patch formation. For the smaller tilt angles the curves exhibit an increase at the beginning of the charge insertion. Then, an equilibrium value is reached whose magnitude is smaller for larger tilt angle. The essential finding is that the transmission remains stable for all tilt angles. Hence, no blocking effects were observed for the FLNR samples of high density, when different tilt angles were used.

Thus, neither the capillary diameter nor the tilt angle are responsible for the significant differences in the blocking effects observed for the two sets of PET capillaries. Rather, in the following, we interpret these differences in terms of the capillary surface conductivities.

3.3. Formation of charge patches

As mentioned, information about the capillary surface conductivities can be obtained from charge patches formed within the capillary. Details about the charge patches are derived from the angular emission of the transmitted ions. The mean emission angle of Ne^{7+} ions ejected in x direction is evaluated as

$$\bar{\theta}_x = \frac{1}{Y_t} \int \theta_x \frac{dY(\theta_x, \theta_y)}{d\Omega} d\Omega \quad (2)$$

Detailed studies of this angle have been performed using FLNR PET capillaries with an areal density of $4 \times 10^6 \text{ cm}^{-2}$ (see in [8,29]). Present results for the tilt angle of 5.3° are shown in Fig. 7(a) indicating strong oscillations, which exceeds the limits

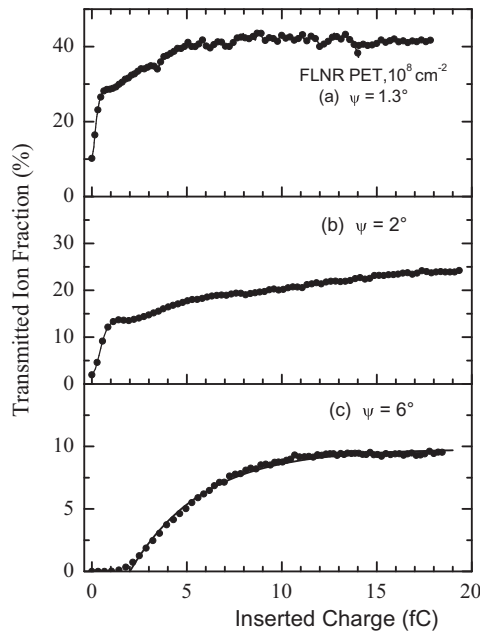


Fig. 6. Fraction f_t of 3-keV Ne^{7+} ions transmitted through FLNR PET capillaries plotted as a function of the inserted charge Q_{in} . The capillary areal density is $1 \times 10^8 \text{ cm}^{-2}$ for all tilt angles of 1.3° , 2° , and 6° as indicated in the graphs.

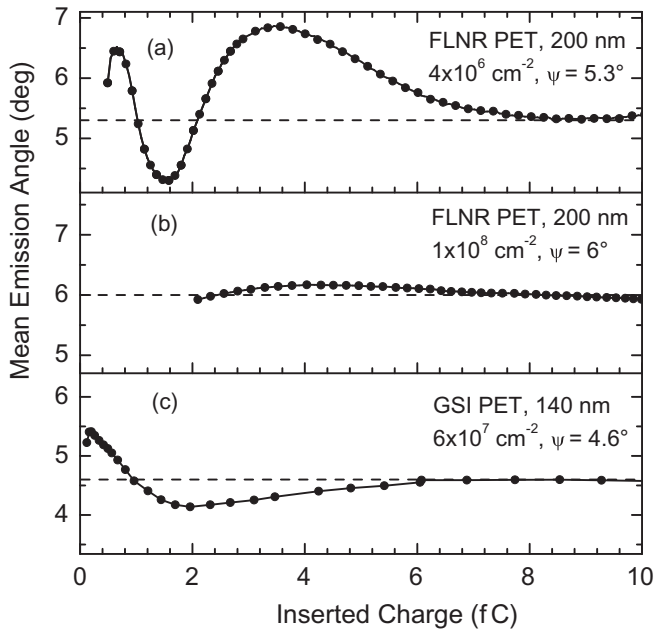


Fig. 7. Mean angle of emission profiles for 3-keV Ne^{7+} as given in Fig. 3. In (a) results for FLNR PET capillaries with a density of $4 \times 10^6 \text{ cm}^{-2}$ are displayed, in (b) results for FLNR PET capillaries with a density of $1 \times 10^8 \text{ cm}^{-2}$ are shown, and in (c) results for GSI PET capillaries with a density of $6 \times 10^7 \text{ cm}^{-2}$ [30] are presented. Capillary diameter and tilt angle are given in each panel. Note the different oscillatory structures.

of $\pm 1^\circ$. The oscillatory structures of the mean angle reveal the formation of transient charge patches partially located within the capillary center region (see also Fig. 1).

For the higher density case, we started from the images in Fig. 3 and evaluated the mean emission angle for the 6° tilt angle by means of Eq. (2). The results are given in Fig. 7(b) indicating that this mean angle is nearly constant in obvious contrast to the oscillatory structure in Fig. 7(a). Recall that both sets of results were

obtained for similar FLNR capillaries. The major difference between the two curves lies in the areal capillary densities, which are $4 \times 10^6 \text{ cm}^{-2}$ and $1 \times 10^8 \text{ cm}^{-2}$ in panel (a) and (b), respectively.

The constant mean angle for the higher capillary density allows for the conclusion that, apart from the entrance charge patch, secondary charge patches are missing in the inner part of the capillary. This finding provides evidence for mechanisms, which inhibit the formation of these transient charge patches. In addition, it is seen that the curve in Fig. 7(b) starts at charge insertion of 2 fC due to the corresponding threshold in the total intensity [Fig. 6(c)]. This relative large threshold indicates a significant delay of the entrance charge patch formation, which again suggests charge depletion mechanisms associated with the high capillary density.

Finally, in Fig. 7(c) we consider the mean emission angle for 3 keV Ne^{7+} ions transmitted through GSI capillaries with the relatively high density of $6 \times 10^7 \text{ cm}^{-2}$. Although less pronounced, noticeable oscillations of the mean angle are observed indicating weaker charge depletion mechanisms so that secondary charge patches can be formed. Moreover, no significant threshold is observed confirming that charge depletion is less important. The observations in Fig. 7 will be associated with effects of neighbor capillaries combined with differences in the conductivities.

4. Discussion and conclusion

In this work, blocking of highly charged ions was studied for PET samples from different laboratories. The blocking is expected to depend on material properties and surface treatments which are partially unknown. However, the experimental results can be interpreted in view of mechanisms affecting the blocking. The strong dependence of blocking effects on the areal capillary density has been explained in model calculations [30] by the influence of the charges accumulated in neighbor capillaries. As the mean distance to the neighbors decreases with increasing capillary density it is evident that neighbor effects are more important for high capillary densities. This interpretation is consistent with the finding that blocking can be avoided when increasing the energy of the incident ions. However, low energies are favorable as guiding is more effective for slow ions. Therefore, it is desirable to find high-density capillaries which do not show blocking at low ion energies.

A major result of the model calculations [30] for 3 keV Ne^{7+} ions was that the charges accumulated in the center area of the neighbor capillaries play the most important role. The charges deposited in the entrance regions of the neighbor capillaries are less influential as they are screened by the metal layer at the sample surface. This explains the experimental observation that blocking effects are more important for capillaries tilted by an angle close to zero degree [11]. For such an angle the charge accumulation is larger in the capillary center than for tilted capillaries, as in the latter case the dominant part of the charge is concentrated in the entrance patch [25].

For the suppression or blocking of ions a noticeable electric field in the z direction along the capillary axis is required. It has been shown by simulations [25] that close to the center the z -field is minor in a single capillary. However, the model calculations [30] provided evidence that neighbor capillaries in close vicinity can produce a significant z -field suppressing the ion transmission. Hence, the strong dependence of the ion blocking on the capillary density, observed for capillaries in PC and PET, has been explained [30]. On the other hand, for the stable transmission through the FLNR capillaries it is expected that the deposited charges are removed during irradiation. An efficient mechanism for charge depletion is the drift along the capillary surface to the conducting metal layers at the capillary entrance and exit [25]. This drift depends on the mobility of the charge carriers at the capillary surface.

The charge drift along the capillary axis is caused by the electric field in the z direction produced by capillary neighbors. The finding that z -field is minor in a single capillary [25] is in accordance with the experimental observation that transient charge patches are created in capillaries of small density, as was concluded from the strong oscillations of the mean emission angle [Fig. 7(a)]. However, since neighbor capillaries can produce a considerable z -field, the secondary charge patches were depleted, as was concluded from the observation that angular oscillations are missing [Fig. 7(b)]. With the removal of charges in the capillary center, the z -field is reduced so that the capillaries become transparent and the observation of stable ion transmission through high density capillaries in FLNR PET may be understood.

The charge transport along the capillary axis requires not only a noticeable z -field but also a significant mobility of the charge carriers. Obviously, the conductivity of the FLNR PET is sufficiently large to provide an efficient charge depletion whereas it is less important for GSI PET capillaries. The weaker charge removal for those capillaries becomes evident from the experimental finding of the oscillatory structures shown in Fig. 7(c). Thus, the essential difference between the PET samples from different laboratories is associated to material properties such as impurities within the bulk and surface treatments. In the past the significant influence of the capillary surface and bulk conductivities was often anticipated but a direct proof was missing [27,28]. Our observations lead to the request that detailed information about the material and its surface treatment should be recorded and provided together with the experimental results.

In conclusion, the present work reveals long-term stable transmission for highly charged neon ions guided through PET nanocapillaries with different areal densities. This observation is in contrast to previous results, which indicated significant blocking effects reported for capillaries in PC and another type of PET. Hence, we conclude that ion blocking is not a general phenomenon for capillaries of high areal density. Rather, blocking and stable transmission depend also on the conductivity of the PET material. This result is favorable for applications of ion guiding through capillaries. In practice, capillaries involving ion blocking are not useful for a longer operation. In this case, stable transmission of guided ions is certainly advantageous. The present results show that it is a challenge to search for materials and surface treatments that inhibit ion blocking effects.

Acknowledgement

We are indebted to Christina Trautmann and Pavel Apel for providing, respectively, the GSI and FLNR capillary foils used in our previous and present experiments. This work was supported by the Hungarian National Science Foundation (OTKA, Grant No. K83886).

References

- [1] N. Stolterfoht, J.H. Bremer, V. Hoffmann, R. Hellhammer, D. Fink, A. Petrov, B. Sulik, *Phys. Rev. Lett.* 88 (2002) 133201.
- [2] N. Stolterfoht, V. Hoffmann, R. Hellhammer, D. Fink, A. Petrov, Z.D. Pešić, B. Sulik, *Nucl. Instrum. Methods Phys. Res. B* 203 (2003) 246.
- [3] N. Stolterfoht, R. Hellhammer, Z.D. Pešić, V. Hoffmann, J. Bundesmann, A. Petrov, D. Fink, B. Sulik, *Vacuum* 73 (2004) 31.
- [4] Y. Kanai, M. Hoshino, T. Kambara, T. Ikeda, R. Hellhammer, N. Stolterfoht, Y. Yamazaki, *Nucl. Instrum. Methods Phys. Res. B* 258 (2007) 155.
- [5] N. Stolterfoht, R. Hellhammer, J. Bundesmann, D. Fink, Y. Kanai, M. Hoshino, T. Kambara, T. Ikeda, Y. Yamazaki, *Phys. Rev. A* 76 (2007) 022712.
- [6] N. Stolterfoht, R. Hellhammer, J. Bundesmann, D. Fink, *Phys. Rev. A* 77 (2008) 032905.
- [7] M. Kreller, G. Zschornak, U. Kentsch, *J. Phys. Conf. Series* 163 (2009) 012090.
- [8] Z. Juhász, B. Sulik, R. Rácz, S. Biri, R.J. Bereczky, K. Tökési, Á. Köver, J. Pálinkás, N. Stolterfoht, *Phys. Rev. A* 82 (2010) 062903.
- [9] D. Li, Y. Wang, Y. Zhao, G. Xiao, D. Zhao, Z. Xu, F. Li, *Nucl. Instrum. Methods Phys. Res. B* 267 (2009) 469.
- [10] N. Stolterfoht, R. Hellhammer, Z. Juhász, B. Sulik, V. Bayer, C. Trautmann, E. Bodewits, A.J. de Nijs, H.M. Dang, R. Hoekstra, *Phys. Rev. A* 79 (2009) 042902.
- [11] N. Stolterfoht, R. Hellhammer, B. Sulik, Z. Juhász, B. Bayer, C. Trautmann, E. Bodewits, R. Hoekstra, *Phys. Rev. A* 83 (2011) 062901.
- [12] Z. Juhász, S.T.S. Kovacs, P. Herczku, R. Rácz, S. Biri, I. Rajta, G.A.B. Gal, S.Z. Szilasi, J. Pálinkás, B. Sulik, *Nucl. Instrum. Methods Phys. Res. B* 27 (2012) 177.
- [13] M.B. Sahana, P. Skog, G. Víkor, R.T. RajendraKumar, R. Schuch, *Phys. Rev. A* 73 (R) (2006) 040901.
- [14] P. Skog, H. Zhang, R. Schuch, *Phys. Rev. Lett.* 101 (2008) 223202.
- [15] S. Mátéfi-Tempfli, M. Mátéfi-Tempfli, L. Piraux, Z. Juhász, S. Biri, É. Fekete, I. Iván, F. Gáll, B. Sulik, G. Víkor, et al., *Nanotechnology* 17 (2006) 3915.
- [16] P. Skog, I.L. Soroka, A. Johansson, R. Schuch, *Nucl. Instrum. Methods Phys. Res. B* 258 (2007) 145.
- [17] Z. Juhász, B. Sulik, S. Biri, I. Iván, K. Tökési, É. Fekete, S. Mátéfi-Tempfli, M. Mátéfi-Tempfli, G. Víkor, E. Takács, et al., *Nucl. Instrum. Methods Phys. Res. B* 267 (2009) 321.
- [18] H.Q. Zhang, N. Akram, P. Skog, I. Soroka, C. Trautmann, R. Schuch, *Phys. Rev. Lett.* 108 (2012) 193202.
- [19] R. Bereczky, G. Kowarik, F. Aumayr, K. Tökési, *Nucl. Instrum. Methods Phys. Res. B* 267 (2009) 317.
- [20] E. Gruber, G. Kowarik, F. Ladening, J.P. Wacławek, F. Aumayr, R.J. Bereczky, K. Tökési, P. Gunacker, T. Schweigler, C. Lemell, et al., *Phys. Rev. A* 86 (2012) 062901.
- [21] T. Ikeda, Y. Kanai, T.M. Kojima, Y. Iwai, T. Kambara, Y. Yamazaki, M. Hoshino, T. Nebiki, T. Narusawa, *Appl. Phys. Lett.* 89 (2006) 163502.
- [22] A. Cassimi, T. Ikeda, L. Maunoury, C.L. Zhou, S. Guillous, A. Mery, H. Lebius, A. Benyagoub, C. Grygiel, H. Khemliche, et al., *Phys. Rev. A* 86 (2012) 062902.
- [23] K. Schiessl, W. Palfinger, K. Tökési, H. Nowotny, C. Lemell, J. Burgdörfer, *Phys. Rev. A* 72 (2005) 062902.
- [24] K. Schiessl, K. Tökési, B. Solleder, C. Lemell, J. Burgdörfer, *Phys. Rev. Lett.* 102 (2009) 163201.
- [25] N. Stolterfoht, *Phys. Rev. A* 87 (2013) 012902.
- [26] N. Stolterfoht, *Phys. Rev. A* 87 (2013) 032901.
- [27] C. Lemell, J. Burgdörfer, F. Aumayr, *Progr. Surface Sci.* 88 (2013) 237.
- [28] N. Stolterfoht, Y. Yamazaki, *Phys. Rep.* 629 (2016) 1.
- [29] N. Stolterfoht, R. Hellhammer, D. Fink, B. Sulik, Z. Juhász, E. Bodewits, H.M. Dang, R. Hoekstra, *Phys. Rev. A* 79 (2009) 022901.
- [30] N. Stolterfoht, R. Hellhammer, B. Sulik, Z. Juhász, V. Bayer, C. Trautmann, E. Bodewits, G. Reitsma, R. Hoekstra, *Phys. Rev. A* 88 (2013) 032902.
- [31] G. Pépy, P. Boeseck, A. Kuklin, E. Manceau, B. Schiedt, Z. Siwy, M. Toulemonde, C. Trautmann, *J. Appl. Cryst.* 40 (2007) s388.
- [32] Y.P. Apel, V. Ovchinnikov, *Rad. Eff. Def. Sol.* 126 (1993) 217.
- [33] S. Biri, J. Vámosi, A. Valek, Z. Kormány, E. Takács, J. Pálinkás, *Nucl. Instrum. Methods Phys. Res. B* 124 (1997) 427.